Pure Appl. Chem., Vol. 79, No. 8, pp. 1383–1402, 2007.
doi:10.1351/pac200779081383
© 2007 IUPAC

Structure, magnetism, and thermodynamics of the novel rare earth-based R_5T_4 intermetallics*

V. K. Pecharsky‡ and K. A. Gschneidner, Jr.

Ames Laboratory of the U.S. Department of Energy and Department of Materials Science and Engineering, Iowa State University, Ames, IA 50011-3020, USA

Abstract: After approximately 30 years of dormancy, the binary, ternary, and multicomponent intermetallic compounds of rare earth metals (R) with the group 14 elements (T) at the R_5T_4 stoichiometry have become a goldmine for materials science, condensed matter physics, and solid-state chemistry. In addition to providing numerous opportunities to clarify elusive structure–property relationships, the R_5T_4 compounds may soon be developed into practical materials by exploiting their unique sensitivity toward a variety of chemical and physical triggers. The distinctiveness of this series is in the remarkable flexibility of the chemical bonding between well-defined, self-assembled, subnanometer-thick slabs and the resultant magnetic, transport, and thermodynamic properties of the R_5T_4 compounds that can be controlled by varying either or both R and T, including mixed rare earth elements on the R-sites and different group 14 (and 13 or 15) elements occupying the T-sites. In addition to chemical means, the interslab interactions are tunable by temperature, pressure, and magnetic field. Presently, a substantial, yet far from complete, body of knowledge exists about the Gd compounds with T = Si and Ge. In contrast, only a little is known about the physics and chemistry of R_5T_4 alloys with other lanthanides, while compounds with T = Sn and Pb remain virtually unexplored.

Keywords: intermetallic compounds; crystal structures; phase relationships; magnetic properties; experimental thermodynamic properties; structure–property relationships.

INTRODUCTION

While the discovery and first use of an intermetallic [1] compound can be traced back to the Bronze Age, the realization of the role this class of materials plays in science and engineering came about much later. To date, some 30 000 individual binary, ternary, and multicomponent intermetallic phases have been prepared and characterized [2]. For many, but not all of them, the crystal structures and, for some, the basic physical and chemical properties have been reported. As the name implies, the majority of intermetallic compounds are metals. Due to predominantly metallic bonding, their crystal structures are often derived by distortions, substitutions, defects, or interstitial insertions starting from two basic lattice variants—hexagonal or cubic—representing close packing of identical, incompressible spheres [3]. On the other hand, numerous intermetallic compounds, especially those formed by semi-metallic group 13 (B, Al, and Ga), group 14 (C, Si, Ge, Sn, and Pb), and group 15 elements (P, As, and Sb), exhibit a tendency toward directionality of chemical bonding. In other words, chemical bonds in intermetallic alloys may have a varying degree of covalency, which in turn may result in low-dimensional and

*Paper based on a presentation at the 19th International Conference on Chemical Thermodynamics (ICCT-19), 30 July to 4 August 2006, Boulder, CO, USA. Other presentations are published in this issue, pp. 1345–1462.

‡Corresponding author

anisotropic interatomic interactions. Although intuitively it is clear that there must be intrinsic and direct relationships between the chemical composition, crystallography, and properties of individual intermetallic compounds, developing an all-inclusive, coherent theory enabling one to easily and reliably predict a new alloy having specific chemistry, crystallography, and bonding, and, by design, exhibiting a given set of physical and/or chemical properties has been a daunting task which is yet to be accomplished.

Rightfully so, intermetallic compounds are considered to be a unique playground for solid-state science, especially because they often form extended families of isostructural or nearly isostructural materials. Here, different chemical elements may occupy identical sites in virtually identical crystal lattices, thus allowing one to examine a balance between chemistry (i.e., the electronic structure of individual components of a compound) and physical properties of a specific, three-dimensional assembly of atoms. Among numerous isostructural intermetallic families, one of the most extensively represented and studied is a series of AB_4 ($AB'_2B''_2$) compounds that crystallize in the $BaAl_4$-type [4] or $ThCr_2Si_2$-type [5] structures. There are well over 700 known representatives of the $AB_4/AB'_2B''_2$ series [2], which is second only to the $MgCu_2$-type [6,7] Laves phase family that has nearly twice as many known members. Strong and lasting interest in the AB_4 and $AB'_2B''_2$ compounds is, to a great extent, related to the discovery of heavy fermion superconductivity in $CeCu_2Si_2$ [8] and recognition that many of the intriguing properties of this and other compounds belonging to the same series are due to their peculiarly *layered* crystal structures. Here, the layering is achieved by stacking flat, square networks built from identical atoms along a four-fold symmetry axis, and it is possible to speculate that both direct and indirect interactions within the monoatomic layers are different from those between the layers. In other words, a layered arrangement of atoms in the intermetallic lattice has been long recognized as a critical factor facilitating a remarkably anisotropic physics.

While many other intermetallic compounds may be classified as layered, the vast majority of the identifiable layers are only one atom-thick, and therefore, they are said to be monolayers. It is worth noting that both the hexagonal and cubic close-packed structures, too, are often treated as different stacking of the familiar close-packed monolayers where each atom has six identical nearest neighbors belonging to the same layer. Yet, every monolayered intermetallic structure remains vastly different from, for example, some other well-known layered materials such as graphite or mica, and as a result, interactions between metallic monolayers are nearly impossible to control without drastically changing their chemistry.

It is much more unusual for an intermetallic alloy to be built from distinct *slabs* that are formed by more than one monolayer of atoms with identifiably strong interatomic interactions between the monolayers belonging to the same slab and usually weaker interactions between the slabs. One such family of intermetallic compounds was discovered in 1966 [9], and one year later [10–12] a total of 13 silicides and 12 germanides of rare earth metals (R) with the R_5T_4 stoichiometry, where T is Si or Ge, had been prepared, isolated, and characterized with respect to their basic structural and, for some of them, their magnetic properties. For more than 30 years after their discovery, interest in these materials remained virtually dormant [13–15] despite two clearly abnormal observations. First was that Gd_5Si_4 orders ferromagnetically some 40 K above the magnetic ordering temperature of pure Gd [12,15], and second was a remarkable difference in the magnetism of apparently isostructural R_5Si_4 and R_5Ge_4 compounds [12]. Only after 1997, when the giant magnetocaloric effect was reported in $Gd_5Si_2Ge_2$ [16], other $Gd_5Si_xGe_{4-x}$ alloys [17], and in a few doped $Gd_5(Si_xGe_{4-x})_{1-y}M_{2y}$ compounds (M = Fe, Co, Ni, Cu, C, Al, and Ga) [18], and when an unusual changeover of materials' chemistry and physics from the silicide to the germanide of Gd was related to distinct differences in their crystal structure that can be traced to a considerable change of specific interatomic interactions [19], the field came alive. As of June 2007, we are aware of 290 published articles authored by researchers from more than 20 different countries in the Americas, Europe, and Asia. The interest in these materials continues to experience a steady growth, i.e., in 2006 and 2007, on the average one paper per week related to vari-

ous aspects of the physics, chemistry, and materials science of the R_5T_4 compounds (R = rare earth or alkaline earth metal, T = Si, Ge, Sn, Ga, In, Sb, and various combinations of these elements) has appeared in print. Being aware that it is impossible to provide a comprehensive description of the current state-of-the-knowledge about the R_5T_4 family in a journal publication, we can only hope that this brief review will result in an even broader interest in these materials by stimulating other scientists from different fields of expertise. As we will show below, so far only the tip of the iceberg has been uncovered and much of the new science lies ahead.

CRYSTALLOGRAPHY AND PHASE RELATIONSHIPS

Today, the crystallography of the R_5T_4 compounds is viewed much differently from what has been assumed in 1967 when the majority of silicides (excluding La_5Si_4, Ce_5Si_4, Pr_5Si_4, and Nd_5Si_4) and all the germanides were assigned to the Sm_5Ge_4-type structure [9,11], even though Smith et al. [10] and Holtzberg et al. [12] noted that the 5:4 silicides may not necessarily be isostructural with the 5:4 germanides despite identical orthorhombic symmetry and similar unit cell dimensions. It is also interesting to note that at that time, the Sm_5Ge_4-type structure was described as a five-layered sequence of monolayers stacked along the longest unit cell edge [10]. In fact, as shown recently by Choe et al. [20], the R_5T_4 compounds are more appropriately described in terms of strongly interacting monolayers forming tightly bound, nearly two-dimensional slabs, as shown in Fig. 1. Because of strong bonding between the monolayers that form the slabs, the latter are remarkably rigid—the slabs undergo negligible changes upon transition from one layered R_5T_4 structure to another. On the other hand, interactions between the slabs vary easily, and therefore, they may be stacked one upon another with different lateral displacements along the a-axis, supporting a surprisingly flexible crystallography, intriguing physics, and in many instances, displacive, martensitic-like structural changes that take place when one or more of the external thermodynamic parameters vary.

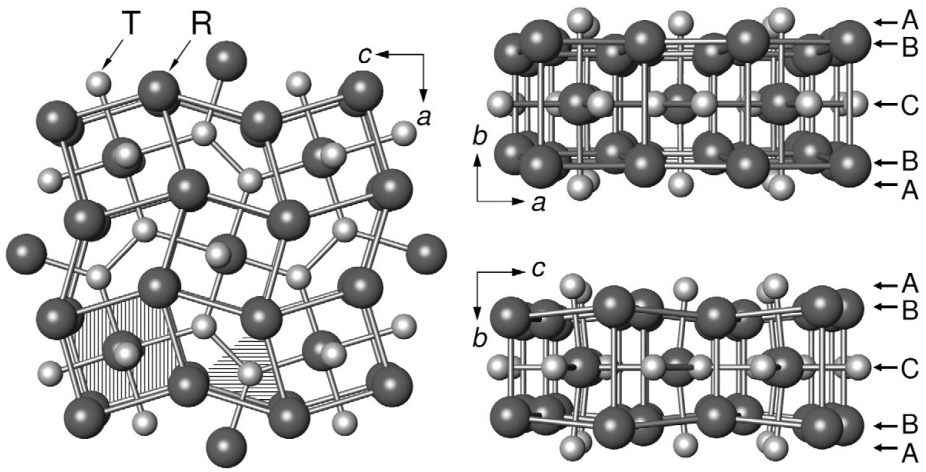

Fig. 1 Pseudo two-dimensional slab, which serves as the building block of the majority of R_5T_4 compounds, shown in three different orientations. The slabs are infinite in the *ac* plane but they are limited to ~7 Å along the *b*-axis. Each slab consists of distorted [R_8] cubes filled with the R atoms and capped with the T atoms (hatched vertically) and from twinned [R_6] trigonal prisms filled with the T atoms, rectangular faces of which are capped with one T and two R atoms (hatched horizontally). It is interesting to note that each slab consists of five monolayers (ABCBA) stacked along the *b*-axis, originally used by Smith et al. [10] to describe the crystallography of the Sm_5Ge_4-type structure. Layers A (only T atoms) and C (R and T atoms) are flat, while layer B (only R atoms) is undulating.

Four distinctly layered structures, known to occur among the R_5T_4 compounds, are illustrated in Fig. 2. In the Gd_5Si_4-type structure (Fig. 2a), the *T*-atoms located on the surfaces of the slabs (i.e., the *T*-atoms from the A layers shown in Fig. 1) form strongly bonded, covalent-like T_2 dimers, thus enabling strong interslab interactions propagating along the *b*-axis. These "short" *T*–*T* bonds are ~2.6 Å long and are shown as thick lines in Fig. 2. The shortest distance between the dimers, i.e., the "long" *T*–*T* distances, is ~5.4 Å, and these are shown as dashed lines in Fig. 2. The Gd_5Si_4-type crystal structure belongs to space group symmetry Pnma, and it is also known in the literature as the O(I)-type structure [19].

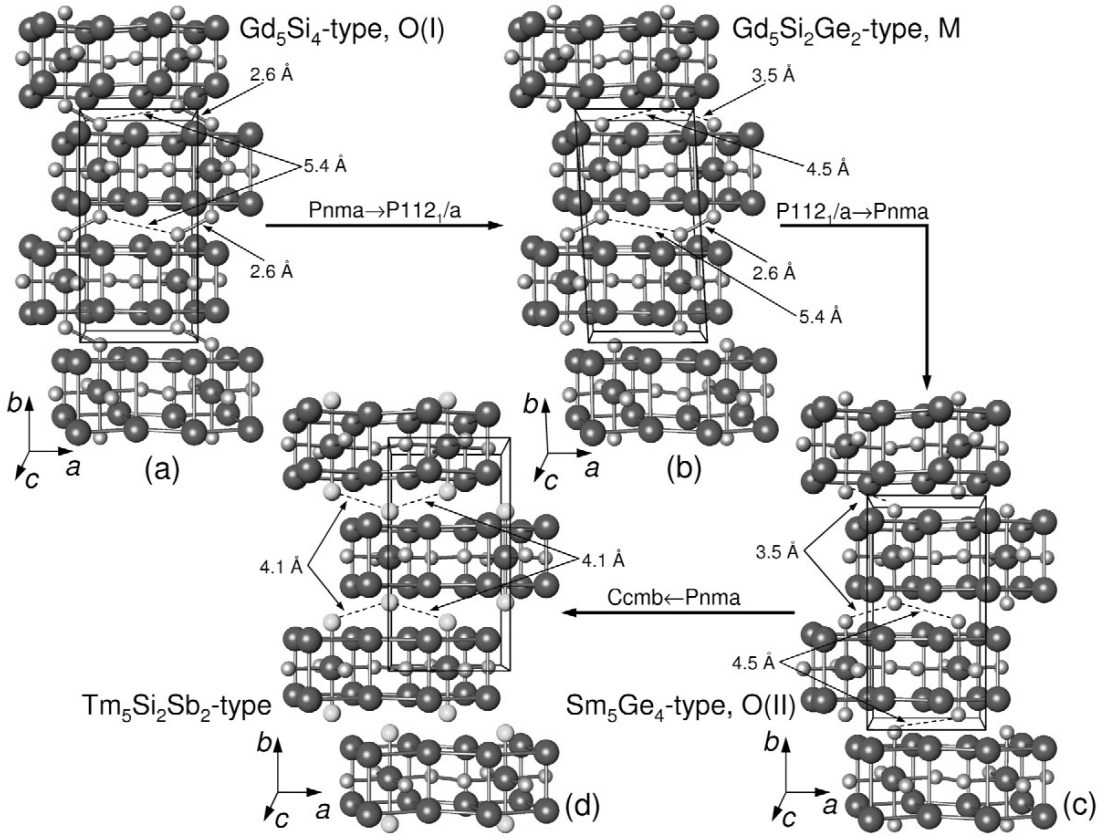

Fig. 2 Four different types of layered structures found among R_5T_4 compounds: (a) the Gd_5Si_4-type structure; (b) the $Gd_5Si_2Ge_2$-type structure; (c) the Sm_5Ge_4-type structure; and (d) the $Tm_5Si_2Sb_2$-type structure. See the text for a description of differences and relationships among these four structure types.

Next is the $Gd_5Si_2Ge_2$-type structure (Fig. 2b), in which the uniformity of the interslab connectivity via the T_2 dimers, and therefore, interslab interactions are much different [19,20]. Here, the strongly bonded T_2 dimers are only found between every other slab, and it is easy to see that interslab interactions similar to those occurring in the O(I)-type structure are now limited to pairs of neighboring slabs. The geometry of the weakly interacting pairs is characterized by better balanced *T*–*T* distances, i.e., ~3.5 and 4.5 Å vs. ~2.6 and 5.4 Å for the short and long interslab *T*–*T* contacts, respectively. The $Gd_5Si_2Ge_2$-type structure belongs to the $P112_1/a$ space group symmetry, and it is also known as the M-type polymorph.

The third in the series is the Sm_5Ge_4-type modification—the one that was actually discovered [10] in 1967—and it is illustrated in Fig. 2c. Here, the uniformity of the interslab interactions is re-

stored, but all of the strongly bonded interslab T_2 dimers are now broken. All short *T*–*T* contacts remain at ~3.5 Å, and the long ones are at ~4.5 Å. The symmetry of this polymorph corresponds once again to space group Pnma, and this arrangement of the slabs is also known in the literature as the O(II)-type structure.

Finally, the fourth structure is the recently discovered $Tm_5Si_2Sb_2$-type [21], which is shown in Fig. 2d. Here, all interslab interactions are also uniform, which is similar to both the O(I)- and O(II)-type structures, but in addition, all the interslab *T*–*T* distances become identical, i.e., ~4.1 Å. This polymorphic modification has the highest symmetry among the four structures, corresponding to space group Ccmb (in this setting, the *a*- and *b*-axes have been switched from the conventional Cmca space group listed in the International Tables for Crystallography). Using the Ccmb space group leaves the crystallographic coordinate system invariant for all four structure types. A few other orthorhombic structures that are intermediate between the O(I) and O(II) types, where the short interslab *T*–*T* distances are longer than the typical 2.6 Å for the O(I) but shorter than the ~3.5 Å found in the O(II), have been reported when Ga is substituted for Ge, i.e., $T = Ge_{1-x}Ga_x$ [22]. All of these phases maintain the Pnma space group symmetry.

The four crystal structures depicted in Fig. 2 are related to one another by shearing neighboring slabs in opposite directions along the *a*-axis by ~0.2 Å each. The three space group symmetries (Ccmb, Pnma, and $P112_1/a$) maintain group–subgroup relationships. It is interesting to note that the $Tm_5Si_2Sb_2$-type structure is only known for electron-rich compounds (i.e., when pentavalent antimony replaces tetravalent Si or Ge), while structures intermediate between O(I) and O(II) types are formed in electron-poor systems (i.e., when trivalent Ga replaces tetravalent Si). Considering the presence of strongly bonded *T*–*T* dimers between the slabs, the O(I)-type structure can be classified as the interslab *T*–*T* bond-rich, while the O(II)- and $Tm_5Si_2Sb_2$-type structures are interslab *T*–*T* bond-poor polymorphs.

To date, the most studied R_5T_4 systems are $R_5(Si_xGe_{4-x})$ alloys, and only a few reports on the crystallography, phase relationships, and properties have been published for the $R_5(Si_xSn_{4-x})$ or $R_5(Ge_xSn_{4-x})$ families [23-34], $R_5(Ge_xGa_{4-x})$ [22,29], $R_5(Si_xSb_{4-x})$ or $R_5(Ge_xSb_{4-x})$ [21,35,36], and $R_5(Ge_xPb_{4-x})$ or $R_5(Ge_xIn_{4-x})$ compounds [29]. A compilation of numerous experimental studies [19,37–58] representing room-temperature crystallography and phase relationships of these materials as a function of composition in the $R_5(Si_xGe_{4-x})$ family is shown in Fig. 3. The Si-rich compounds formed by light lanthanides (La, Ce, Pr, and Nd) adopt the tetragonal Zr_5Si_4-type structure [59]. The latter contains no slabs, nor is it layered despite being intimately related [60] to each of the four structure types shown in Fig. 2. All pseudobinary mixed silicide-germanide systems except *R* = Y, La, Yb, and Lu, exhibit at least three different types of the crystal structures as the Si to Ge ratio varies from $x = 4$ to $x = 0$. Furthermore, when *R* = Yb and Lu, these phases have only one structure across the pseudobinary R_5Si_4–R_5Ge_4 binary systems (see below). Almost all germanides adopt the O(II)-type structure, which has the largest unit cell volume compared to the M (intermediate unit cell volume) and the O(I) (the smallest unit cell volume) crystallographic modifications. As the concentration of Si increases, the O(II)-type structure is replaced with the M-type polymorph which appears in almost every $R_5Si_xGe_{4-x}$ system. The M-type structure is substituted by the O(I)-type (or Zr_5Si_4-type) structure at high Si concentrations. It is interesting to point out that the M-type structure is stable in the vicinity of equiatomic Si to Ge ratios for *R* from Ce to Gd, but its stability region systematically shifts to Ge-poor concentrations from Gd to Er, and presumably, for Ho and Tm. Considering that replacing Ge by Si and vice versa has no effect on the average valence electron concentration, the observed structural transitions are likely driven by the varying phase volume. Thus, replacing larger Ge atoms by the smaller Si atoms is, in a way, equivalent to increasing the chemically induced pressure, which destabilizes a high-volume O(II) polymorph, transforming it into a smaller volume M-phase, and finally, into the smallest volume O(I)-type structure. The chemical pressure argument also holds well for the light lanthanide R_5T_4 systems because the tetragonal Zr_5Si_4-type alloys are low-volume phases compared to the corresponding O(II)- and M-type compounds.

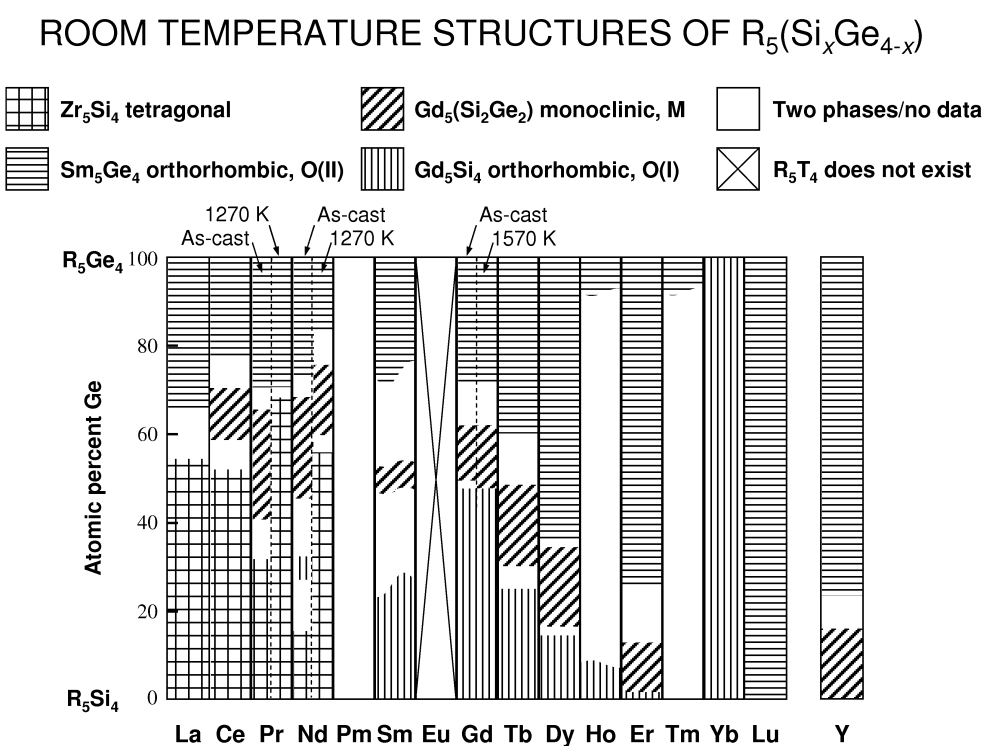

Fig. 3 Phase relationships and room-temperature crystallography of $R_5Si_xGe_{4-x}$ phases. Straight phase boundaries designate terminal compositions that have been established with a few mol % accuracy, while curved boundaries designate terminal compositions known to ~25 mol % (usually based on examination of alloys with x = 4, 3, 2, 1, and 0).

Of the few $R_5Si_xGe_{4-x}$ systems studied both in the as-cast and heat-treated conditions, annealing between 1170 and 1770 K has a considerable effect on phase stability around x = 2 when R = Gd [43,61–63]. Thus, it is not uncommon to find a mixture of O(I) and M phases in the as-cast alloys, especially when using relatively low-purity, so-called 99.9 % Gd [64], while appropriate heat treatment results in the transformation of the O(I) impurity into the thermodynamically stable M-$Gd_5Si_xGe_{4-x}$. This phenomenon is in part related to concentration gradients with respect to Si and Ge ratio that develop spontaneously during solidification with Si-rich grains adopting the O(I)-type structure (also see next section regarding the role of interstitial oxygen in the stabilization of the high-temperature O(I) phase). In addition to homogenization, high-temperature heat treatment of $Gd_5Si_2Ge_2$ results in a partial ordering of the crystal structure via a redistribution of Si and Ge atoms [62]. While in the as-cast alloys, the Si and Ge atoms occupy the corresponding lattice sites nearly randomly, a tendency toward enrichment of the sites responsible for the interslab bonding in Ge is observed upon annealing. These changes produce a sharper magnetic ordering/disordering transformation and result in a small but detectable reduction of the phase-transformation temperature [62]. Heat treatment appears to have a much more pronounced effect on phase relationships in some of the light lanthanide-containing systems. Thus, the extent of phase fields and even the presence of the M- and O(I)-type phases are considerably changed by annealing at 1270 K when R = Pr and Nd, see Fig. 3 [44,45,47,50]. We believe that these changes with heat treatment reflect the complexity of the corresponding equilibrium-phase diagrams and are related to a small difference between the chemical potentials of Si and Ge and resulting minuscule driving forces that preclude the completion or even the occurrence of some phase transformations during a relatively quick solidification and cooling typical for small (1–15 g) arc-melted alloy buttons.

Furthermore, the major annealing effects observed in the systems with Pr and Nd compared to the system with Gd (Fig. 3) correlate with different purities of the rare earth elements used to prepare the alloys. While most of the work with R = Gd has been done using high-purity rare earth metal (better than 99.8 at % or 99.95 wt % Gd with respect to all other elements), the 99.9 % pure (with respect to the other rare earths only) Pr and Nd employed in refs. [44,45,47,50] may have contained as much as 0.5 to 1 at % of carbon and/or oxygen [64]. On one hand, high-temperature anneals promote segregation of oxides on grain boundaries, thus lowering oxygen concentration inside the grains, but on the other hand carbon is expected to be redistributed more evenly throughout the alloy, which may explain drastic changes in the phase stability in the $Nd_5Si_{4-x}Ge_x$ and $Pr_5Si_{4-x}Ge_x$ systems. Future systematic studies employing high-purity rare earth metals with controlled amounts of interstitial impurities are highly desired.

The systems with R = Yb and Lu clearly exhibit anomalous behavior since only one structure—the O(I) or the O(II) polymorph, respectively—is observed over the whole range of concentrations. On one hand, the stability of the O(II)-type structure when R = Lu is expected from the systematic structural changes observed from R = Gd to R = Lu, and this gradual transformation may be explained by conventional geometrical factors (effect of chemical pressure), recalling that Lu is the smallest of all lanthanides [52]. The system with Y, where pure Y_5Si_4 retains the M-type structure, then fits the general trend for the heavy lanthanides assuming that the effective atomic radius of Y in R_5T_4 compounds is between that of Er and Lu. On the other hand, the anomaly when R = Yb is related to electronic effects, i.e., to the stability of Yb^{2+} valence state [53,65]. Hence, when divalent Yb replaces trivalent R, the valence electron concentration in $Yb_5Si_xGe_{4-x}$ is lowered compared to other $R_5Si_xGe_{4-x}$ compounds. This substitution has a similar effect on the crystallography of R_5T_4 materials as when tetravalent Ge is replaced by trivalent Ga in $Gd_5Ge_{4-x}Ga_x$ [22,66]. As the concentration of Ga increases, the O(II)-type structure adopted by the pure germanide is replaced by the O(I)-type lattice when x = 2. The structural behavior exhibited by the $Yb_5Si_{4-x}Ge_x$ system confirms that low valence electron count results in the stabilization of strong interslab T–T dimers. The volume argument considered above suggests that the large-volume O(II) phase would be the equilibrium phase and not the low-volume O(I) Gd_5Si_4-type observed in the $Yb_5Si_xGe_{4-x}$ pseudo-binary system, which indicates that the electronic concentration dominates the volume factor in deciding which crystal structure is formed. The valence electron concentration argument correlates well with an independent observation that increasing the valence electron count when some of the Ge atoms are replaced by Sb results in the complete elimination of the interslab dimers by stabilizing the $Tm_5Si_2Sb_2$-type structure in $Gd_5Ge_{4-x}Sb_x$ at x = 2 [36]. These observations highlight the importance of this chemical tool in tuning the crystallography, and therefore, the physical properties of R_5T_4 materials.

REPRESENTATIVE CRYSTAL STRUCTURE–MAGNETIC PROPERTY RELATIONSHIPS AND THE THERMODYNAMICS OF R_5T_4 SYSTEM

Systematic variations of the crystal structure with composition described in the previous section bring about systematic changes of the physical properties of these intermetallic compounds, which is illustrated in Fig. 4 in the form of the magnetic and structural phase diagram of the $Gd_5Si_xGe_{4-x}$ system [17,37,43,63,67]. Compounds with x between ~2 and 4 that adopt the interslab T_2 dimer-rich O(I)-type structure in the paramagnetic (PM) state order magnetically via a conventional second-order phase transformation at temperatures higher than closely related compounds with x < ~2 that have the interslab T_2 dimer-poor M and O(II) structures. Furthermore, the Curie temperatures of the PM O(I)-type compounds (T_C > 300 K) are higher than that of the elemental Gd (T_C = 294 K), indicating the enhancement of exchange interactions despite a 55:45 (atomic) dilution of Gd with nominally nonmagnetic Si and Ge. All of the alloys in this phase region exhibit a weak, nearly linear dependence of their Curie temperatures on composition with $dT_C/dx \cong 20$ K. This gradual reduction of the Curie temperature from ~336 to 300 K is consistent with a gradual increase of the phase volume (Fig. 5) and elongation of inter-

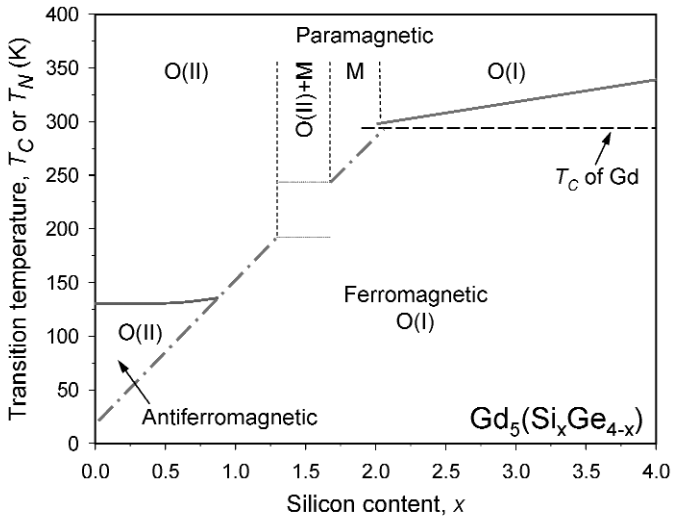

Fig. 4 Spontaneous magnetic ordering temperatures of $Gd_5Si_xGe_{4-x}$ compounds as functions of Si concentration, x. The thick solid lines delineate boundaries of the second-order phase transitions, and the thick dash-dotted lines delineate the same for the first-order phase transformations. The two thin horizontal lines between $x = 1.3$ and $x = 1.6$ indicate constant temperatures of FM-O(I) → PM-M and FM-O(I) → PM-O(II) transformations in the region where the crystal structures of the PM phases are different, i.e., a two-phase region. The Curie temperature of pure Gd metal (thin dashed line) is shown for reference purposes.

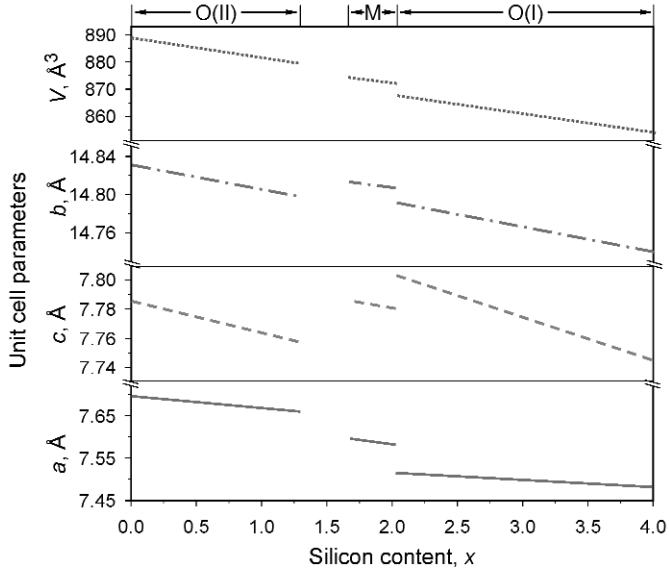

Fig. 5 Unit cell dimensions and phase volume of the phases formed in the $Gd_5Si_xGe_{4-x}$ system at room temperature as functions of Si concentration, x. Note the change in the scales for the lattice parameters.

atomic distances with increasing Ge content. When x falls below 2, the crystal structure of the PM $Gd_5Si_xGe_{4-x}$ changes from the O(I)- to the M-type polymorph. This structural modification in the PM state has a considerable effect on the spontaneous magnetic ordering temperature (Fig. 4): in addition to dropping below the Curie temperature of the elemental Gd, the T_C of these alloys becomes strongly

dependent on the composition. dT_C/dx increases more than six-fold, from ~20 to 130 K, even though phase volume keeps rising with decreasing x at practically the same rate as in the O(I) phase region (Fig. 5). Thermodynamically, this PM–ferromagnetic (FM) transition becomes a first-order transformation because it overlaps with a structural change between the M- and O(I)-types of crystal structures. Finally, when $0 \le x < \sim 1.3$, the PM $Gd_5Si_xGe_{4-x}$ alloys adopt the O(II)-type structure. Here, dT_C/dx stays nearly identical to that of the M-phase, and the boundary separating the FM-ordered phase from either the PM or antiferromagnetic (AFM) state remains a first-order phase transition. Below $x \cong 0.9$, the alloys initially order AFM with a nearly compositionally independent Néel temperature, i.e., $T_N \cong 130$ K. Furthermore, they retain the O(II) structure in the AFM state, and this magnetic ordering transition is second-order (Fig. 4). Similar dependencies of the magnetic properties on chemical composition and crystallography have been reported for R = Pr [47] and R = Tb [41]. A large change in the a-lattice parameter and minimal changes in the b- and c- directions (see Fig. 5) that accompany the sheer distortions in the O(I) → M → O(II) phase sequence (see Fig. 2) when x changes from 4 to 0 point to the existence of slabs in these intermetallic systems.

Regardless of x, the ground state of the $Gd_5Si_xGe_{4-x}$ system is O(I)-FM phase, i.e., it appears to be structurally and magnetically homogeneous over the whole range of concentrations, unlike the PM state, which has three structurally distinct phase regions. From the little that we know about the microscopic magnetism of these Ge-rich compounds, based on both the bulk magnetic measurements [68–71] of single crystals and X-ray resonant magnetic scattering [72], the O(I)-FM state may not, however, be completely magnetically homogeneous since the easy magnetization direction changes from parallel to the a-axis for $x = 1.7$ and $x = 2$ to the b-axis when $x = 0$. Furthermore, as follows from temperature-dependent, low magnetic field measurements of $Gd_5Si_{1.7}Ge_{2.3}$ and $Gd_5Si_2Ge_2$ single crystals [68,70,73], the easy magnetization direction in the ferromagnetically ordered state is temperature-dependent.

Below, we illustrate the intricate interplay of structure, magnetism, and thermodynamics of the R_5T_4 system by using only two representative examples—$Gd_5Si_2Ge_2$ and Gd_5Ge_4.

$Gd_5Si_2Ge_2$

First principles calculations, which to date are nearly exclusively concerned with $Gd_5Si_2Ge_2$ [63,74–80], indicate that bonding and crystallography play a major role in defining the magnetic properties of this and other R_5T_4 compounds. Thus, breaking and reforming of the interslab T_2 dimers, which accompanies the O(I)-M structural transition, and the related ~0.9 Å elongation and contraction, respectively, of the interslab T–T bonds affects both the location of the Fermi level and the effective magnetic exchange coupling, J_0. Comparing the FM-ordered O(I)-$Gd_5Si_2Ge_2$ with the hypothetical FM M-$Gd_5Si_2Ge_2$, the former is characterized by larger magnetic moments of the individual Gd atoms (the difference arises from the varying contribution from the 5d electrons of Gd), a larger J_0, and a lower total energy (at 0 K) than the latter, thus explaining the stability of the O(I)-type structure in the ferromagnetically ordered state. As shown in Fig. 6, the temperature of the magnetostructural transition, T_C, and its first-order nature in $Gd_5Si_2Ge_2$ are reproduced quite well by using the tight binding linear muffin tin orbital (TB-LMTO) method within the framework of the local spin density approximation with the Coloumb correlation parameter (LSDA+U) together with magnetothermodynamic models [80]. Here (the lower part of Fig. 6, left-hand scale), the predicted FM ordering temperatures of the O(I)- and M-type $Gd_5Si_2Ge_2$ phases are $T_C^{O(I)} = 301$ K and $T_C^{M} = 209$ K, respectively. Each of the phases should order ferromagnetically via a second-order transformation typical for magnetic order–disorder transitions. However, when PM M-$Gd_5Si_2Ge_2$ is cooled, its free energy remains lower than that of both the PM and FM O(I)-$Gd_5Si_2Ge_2$ below the Curie temperature of the latter (the upper part of Fig. 6, right-hand scale). Hence, when the free energies of the two polymorphs become equal at T_C, the O(I)-$Gd_5Si_2Ge_2$ phase is already well below its $T_C^{O(I)}$. As a result, the polymorphic transition at T_C also involves FM ordering with a large, discontinuous increase of the spontaneous magnetization, as is also shown in Fig. 6 by a thick solid line. As one can see from the experimental values of the spontaneous

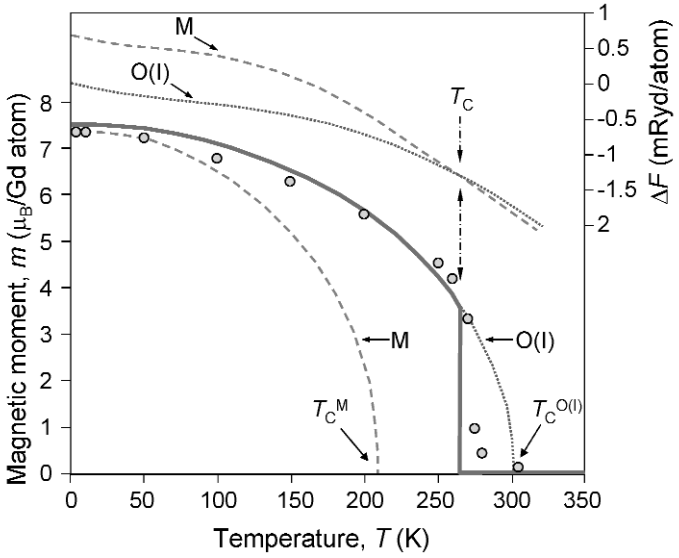

Fig. 6 Spontaneous magnetization as a function of temperature (lower part, left-hand scale) and Helmholtz free energy (upper part, right-hand scale) of M-$Gd_5Si_2Ge_2$ (dashed lines) and O(I)-$Gd_5Si_2Ge_2$ (dotted lines) calculated from first principles. At the magnetostructural transition temperature, T_C, the FM-ordered O(I)-$Gd_5Si_2Ge_2$ transforms into M-$Gd_5Si_2Ge_2$ which must be already PM at T_C, thus resulting in a discontinuous change of the magnetization. The thick solid line follows the magnetization of the system as temperature varies. The solid circles represent the experimental values of the spontaneous magnetization of $Gd_5Si_2Ge_2$.

magnetization (data points in Fig. 6), the agreement between the theory and experiment is nearly quantitative.

Since the transformation at T_C causes remarkable changes in both the crystallography and magnetism of $Gd_5Si_2Ge_2$ and related compounds, it is easily controlled by magnetic field in addition to more conventional thermodynamic triggers of temperature and pressure. Thus, the giant magnetocaloric effect [16–18], colossal magnetostriction [61,70], and giant magnetoresistance (MR) [83–88] are always observed when the magnetic field applied above T_C initiates PM-M $\rightarrow$ FM-O(I) transformation. In addition to these magnetic-field-induced phenomena, other anomalous behaviors have been reported when either the temperature or magnetic field cause the same magnetostructural transition. These include spontaneously generated voltage [89,90], training effects [87,91–94], unusual transformation dynamics [93,95–99], abnormal thermal effects [100], strong acoustic emissions [101], and arrested kinetics leading to an unconventional glassy state [102].

In addition to the low-temperature magnetostructural transformation described above, $Gd_5Si_2Ge_2$ and other compounds with $x \cong 2$ exhibit a purely structural, high-temperature phase transformation around 600 K [63,81,82] between M (low-temperature) and O(I) (high-temperature) polymorphs, both of which are PM. Unlike the low-temperature magnetostructural transition, which is sharp and quickly proceeds to near completion, the high-temperature M-PM $\rightarrow$ O(I)-PM transformation is sluggish [63]. Most interestingly, the high-temperature O(I)-PM $Gd_5Si_2Ge_2$ can be retained below 600 K by quenching. This feature opens an opportunity to examine the effects of the crystallography on the magnetic and other physical properties of an intermetallic system. Even though a recent report [82] indicates that the stability of the O(I)-PM $Gd_5Si_2Ge_2$ near room temperature may be related to a small amount of interstitial oxygen absorbed by the compound at high temperatures, the effects of oxygen impurity on the electronic structure of O(I)-PM $Gd_5Si_2Ge_2$ are nearly negligible [82], and therefore, these small changes in the impurity content have little to no effect on physical properties compared to a tremendous change of the crystallography.

Thus, when the $Gd_5Si_2Ge_2$ compound adopts the M-type structure in the PM state, its properties clearly reflect the presence of the magnetostructural, first-order phase transformation that occurs at T_C = 268 K in a zero magnetic field, see Figs. 7a and 8a. The behavior of the magnetization as a function of magnetic field, shown in Fig. 7a, is indicative of a hysteretic, metamagnetic-like transition between the PM and FM states. The heat capacity, Fig. 8a, exhibits a sharp peak due to a FM ordering–disordering transition coupled with a structural transformation between O(I) and M polymorphs [20,61,103]. The peak is only slightly broadened by the magnetic field, while its temperature increases nearly linearly with the increasing field with a rate of 0.56 K/kOe, indicating that even in a 100 kOe field the transformation remains first-order, and the magnetic and crystallographic changes remain coupled. On the other hand, when the O(I) $Gd_5Si_2Ge_2$ polymorph is stable in the PM state, its magnetic and thermodynamic properties are considerably different from the PM M phase (compare Figs. 7b and 8b with 7a and 8a, respectively). The transition at T_C = 301 K (note that this experimental value is a perfect match to the theoretical prediction, see Fig. 6 and relevant discussion above) is a second-order transformation (Fig. 8b), which is typical for the vast majority of magnetic ordering–disordering transformations. The applied magnetic field broadens the heat capacity peak and shifts the magnetic entropy toward higher temperatures, which is also representative of a majority of conventional FM materials. The isothermal magnetization behavior also becomes characteristic of "standard" ferromagnetism, exhibiting no hysteresis (Fig. 7b). All of these differences are due to the fact that when the PM O(I)-$Gd_5Si_2Ge_2$ orders ferromagnetically, the ordering is not coupled with a change in the crystal lattice, as was the case with the M-PM $Gd_5Si_2Ge_2$.

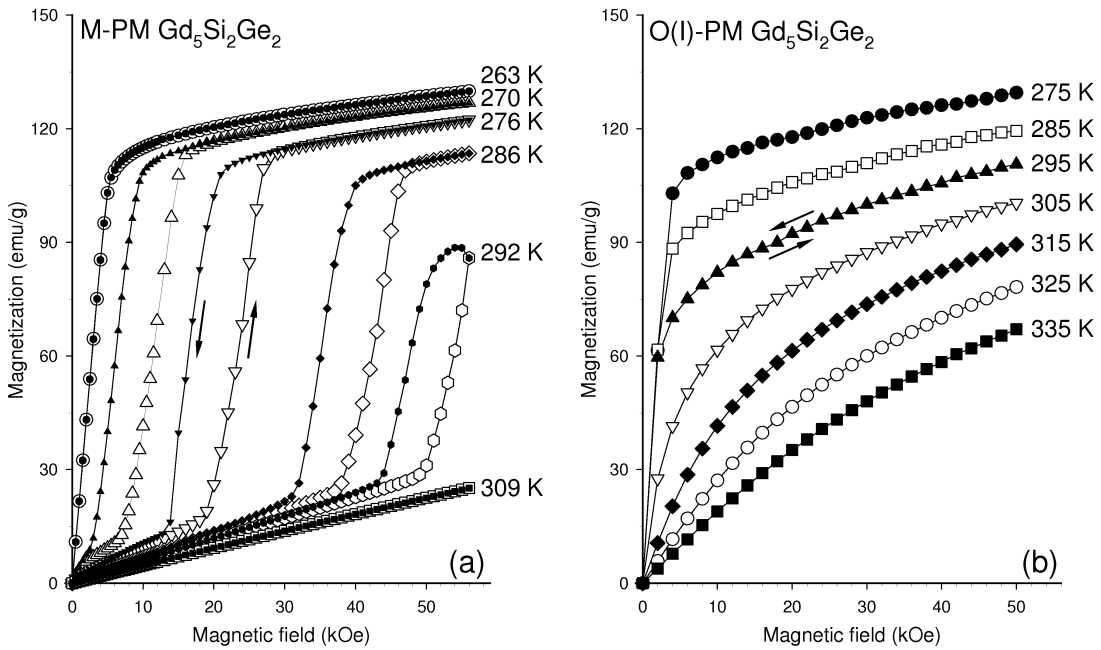

Fig. 7 The isothermal magnetization of the two polymorphic modifications of $Gd_5Si_2Ge_2$ vs. the applied magnetic field in the vicinity of T_C: (a) the monoclinic PM polymorph and (b) the orthorhombic PM polymorph. The field-increasing branches in (a) are shown using large open symbols, and the corresponding field-decreasing branches using small filled symbols.

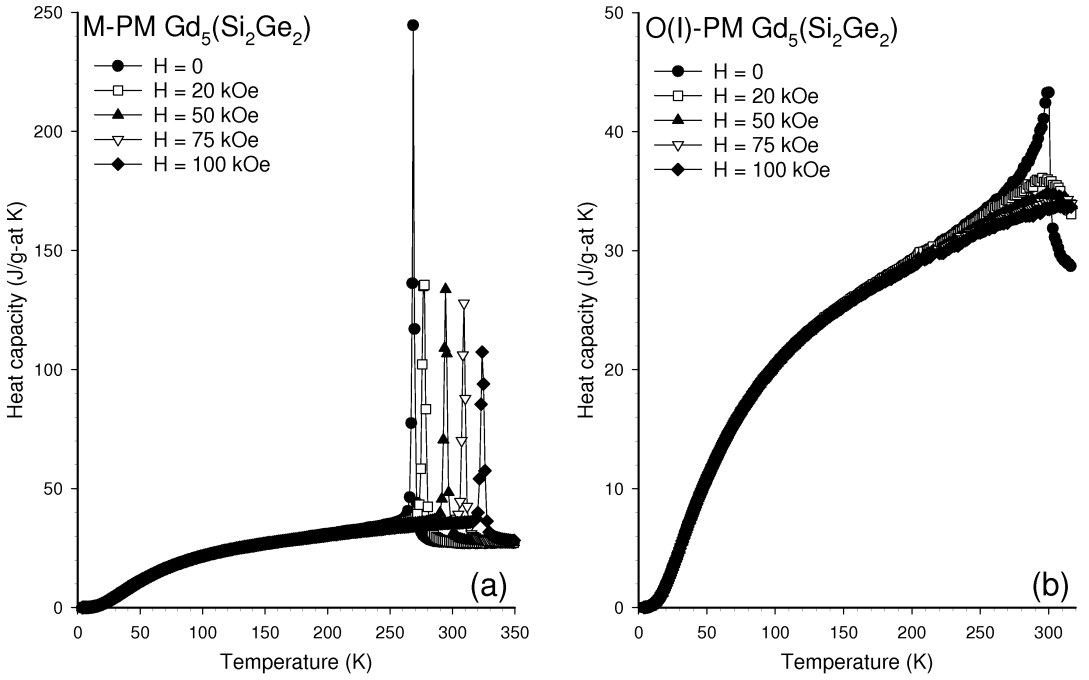

Fig. 8 The heat capacity of the two polymorphic modifications of $Gd_5Si_2Ge_2$ measured as a function of temperature in constant magnetic fields: (a) the monoclinic PM polymorph and (b) the orthorhombic PM polymorph.

This crystallographic flexibility, and therefore, the ability to alter crystal structure without changing the materials' chemistry is especially important when it is of interest to separate the contributions from the two sublattices (magnetic and crystalline) into any effect that is caused by the application of magnetic field. Thus, it has been shown experimentally [103] and theoretically [80] that as much as ~70 % of the isothermal magnetic intropy change in low magnetic fields (20 kOe or less) originates from the lattice. Even in stronger magnetic fields (50 to 100 kOe), the role of the lattice in the magnetocaloric effect remains substantial, although its relative contribution decreases from 52 % (ΔH = 50 kOe) to 40 % (ΔH = 100 kOe) because the lattice contribution [the molar entropy of the O(I)-M transformation is ΔS_{st} = 1.1 J mol(atoms)$^{-1}$ K^{-1}] remains magnetic-field-independent [103,104], while the contribution to the magnetocaloric effect from the magnetic sublattice scales with the magnetic field [105].

Interestingly enough, both experimental and theoretical studies of the magnetoresistance (MR) of $Gd_5Si_2Ge_2$ [78] indicate some dependence on the type of the magnetic order but the anisotropy of the MR does not. The anisotropy of the MR in $Gd_5Si_2Ge_2$ arises nearly exclusively from the structural M-O(I) transition taking place concurrently with the FM ordering at T_C because of (1) drastic changes in the lattice occur along the *a*-axis (see Figs. 2a,b), and (2) interactions between the slabs along the *b*-axis are greatly affected by the variability of the *T*–*T*, Gd–Gd, and Gd–*T* interslab bonds. Combined, these changes in this layered crystal structure result in the largest MR along the *a*- and *b*-axes, while the MR along the *c*-axis is the smallest. Together with other experimental and theoretical evidence (e.g., enhanced effective FM exchange parameter in the interslab bond-rich O(I)-type structures compared to the interslab pond-poor O(II)- and M-type structures [63]), this result supports the validity of representing the crystallography of the R_5T_4 family as different stacking of identical slabs despite the dominance of metallic bonding in these systems.

Gd_5Ge_4

One of the parent compounds in the $Gd_5Si_xGe_{4-x}$ system—the binary Gd_5Ge_4—is especially interesting because unlike the ternary mixed germanide-silicides, in which the *T*-sites are populated by both Si and Ge atoms with a marked preference of the Si atoms for the intraslab sites (the C in Fig. 1) and the Ge atoms preferably occupying the interslab positions (the A layers in Fig. 1) [20,106], it lacks the intrinsic Si/Ge disorder on the *T*-sites. The observed peculiar magnetic properties of Gd_5Ge_4 are clearly related to instability of its crystal structure. Furthermore, it appears that the unusual magnetic correlations in Gd_5Ge_4 originate from the anisotropy of exchange interactions that arises from the presence of the distinctly two-dimensional slabs exhibiting varying interslab interactions.

Thus, the magnetic ground state of Gd_5Ge_4 is AFM [88,97,107–111], see Fig. 4. As follows from bulk magnetization measurements of a single crystal [69] and microscopic data obtained from X-ray magnetic resonant scattering [72], the individual slabs order ferromagnetically with the net FM moment along the *c*-axis, but the coupling between the slabs is AFM (Néel temperature, T_N = 128 K), as shown schematically in Fig. 9. This indicates that the intraslab exchange interactions are strong, while the interslab exchange interactions in the *T*–*T* bond-poor O(II) structure are weak. The AFM state can be transformed into the FM state depending on the temperature and the applied magnetic field as long as the latter exceeds ~10 kOe. At the same time, the crystal structure transforms from the O(II)-type to the *T*–*T* bond-rich O(I)-type polymorph, with the transition showing a martensitic-like character [104,112,113]. It appears that the restoration of strong *T*–*T* bonds between the slabs results in considerably strengthened interslab exchange interactions.

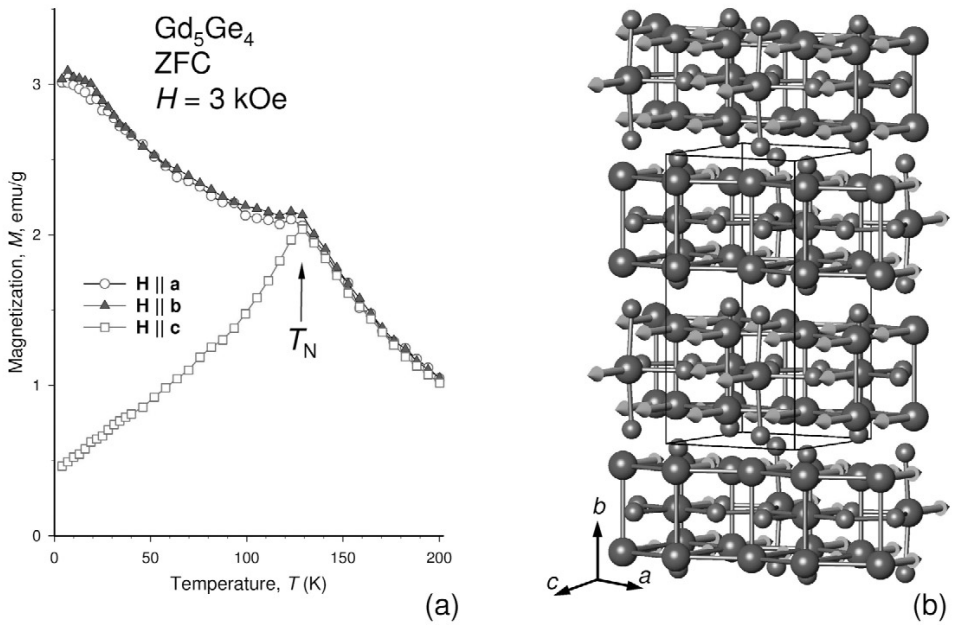

Fig. 9 The magnetization of Gd_5Ge_4 single crystal measured with the magnetic field vector (**H**) parallel to each of the three principal crystallographic directions (a) and the schematic of the microscopic magnetic structure of Gd_5Ge_4 inferred from both the bulk magnetization and X-ray magnetic resonant scattering measurements (b). The magnetization data were collected on warming in a 3 kOe magnetic field after cooling the sample to the lowest temperature of each measurement in a zero field.

Unlike any other member of the R_5T_4 family studied so far, the germanide shows a remarkable change in the reversibility of the magnetostructural transformation at low temperatures. As shown in Figs. 10a–c, below ~10 K, the magnetic-field-induced AFM–FM transition in a polycrystalline Gd_5Ge_4 is irreversible, while above ~20 K it becomes completely reversible. Between ~10 and ~20 K, there exists a mixture of states and the material exhibits both irreversible and reversible AFM–FM transformations [100,108,114]. These drastic changes in the magnetization behavior are nearly precisely followed by significant changes in the crystallography and phase composition. The molar concentration of the O(I) Gd_5Ge_4 (Fig. 10d) increases rapidly between ~15 and 20 kOe, just as the bulk magnetization (Fig. 10a) does at the same temperature. Also, the irreversibility of the magnetization behavior at 6.1 K (Fig. 10a) is followed by the irreversible structural transformation from O(II) Gd_5Ge_4 to the O(I) polymorph, which is clearly seen in both the phase contents (Fig. 10d) and the unit cell dimensions of the majority phase (Fig. 10e). The behavior illustrated in Figs. 10a–e was recently explained [102] by assuming that in addition to the O(II) AFM–O(I) FM phase transformation boundary (hatched horizontally in Fig. 10f), there exists a freezing/unfreezing, glass-like transition, whose boundary is hatched vertically in Fig. 10f. The presence of this additional, glass-like transition renders the material completely or partially kinetically arrested in low magnetic fields at temperatures lower than ~40 K. Thus, when Gd_5Ge_4 is zero-field-cooled to 6.1 K and then the magnetic field is increased to 30+ kOe (Figs. 10a,d,e) the system remains kinetically arrested in fields up to ~14 kOe, at which the magnetic-field-induced O(II) AFM → O(I) FM transformation would have been completed without the arrest. Between ~14 and 16 kOe, the system, which is still in the glass-like state, retains the metastable O(II) AFM state. A sharp transformation is observed for both the magnetic and crystal structures as soon as the system reaches the unfreezing boundary (Figs. 10a,d, respectively). The transformation then proceeds gradually across this boundary and is completed above ~26 kOe. When the magnetic field is now reduced isothermally, the O(II) FM Gd_5Ge_4 first crosses the same freezing boundary, thus approaching the O(I) FM → O(II) AFM transition boundary in a glassy, kinetically arrested state, which makes a reverse transformation impossible. As a result, Gd_5Ge_4 retains the O(I) FM state and the magnetic-field-induced transformation is completely irreversible at this temperature. When the same magnetic field cycle is repeated at 14.4 K, the phase transition and (un)freezing boundaries overlap, resulting in a partial preservation of the metastable O(I) FM Gd_5Ge_4 when the field is cycled back to zero. Finally, when the magnetic field is cycled at 29 K, the freezing boundary does not interfere with the magnetostructural phase transition regardless of the direction of the magnetic field change. In addition to varying reversibility, this picture explains the unusually sharp field-induced discontinuities of the magnetization observed in zero magnetic-field-cooled samples as the temperature drops below ~8 K (see Fig. 10a in this work, Fig. 5 in ref. [114], and Figs. 1 and 3 in ref. [108]): as the O(II) AFM phase moves further and further away from equilibrium when the temperature is lowered, increasing the magnetic field results in a sharper and sharper AFM–FM transformation because of the larger driving force due to a progressively larger ΔG.

High-temperature anomalies of magnetic properties of Gd_5Ge_4 have been reported in the past. They include nonlinear inverse magnetic susceptibility below ~230 K, possibly indicating some kind of an ordering process [107], and breaking of the long-range AFM ordering by magnetic fields higher than ~130 kOe [111]. The most interesting anomalies, however, are observed in low magnetic fields. As follows from the low-magnetic-field properties of a single crystal of Gd_5Ge_4 [115], in addition to the interplay between reversibility and irreversibility of the magnetostructural transformation, the system exhibits complex relationships between long- and short-range magnetic order. Dynamic short-range FM clustering is observed between 70–80 K and T_N = 128 K. While the static FM component adopts the O(I)-type structure, it appears that the dynamic FM clusters maintain the O(II)-type crystal structure, which is the same as for the AFM matrix. Above T_N = 128 K but below T_G = 240 K, a different type of short-range FM correlations and dynamic FM clustering, which may be attributed to the Griffiths phase-like [116] state of Gd_5Ge_4, is also observed The latter is quite similar to the Griffiths-like phase

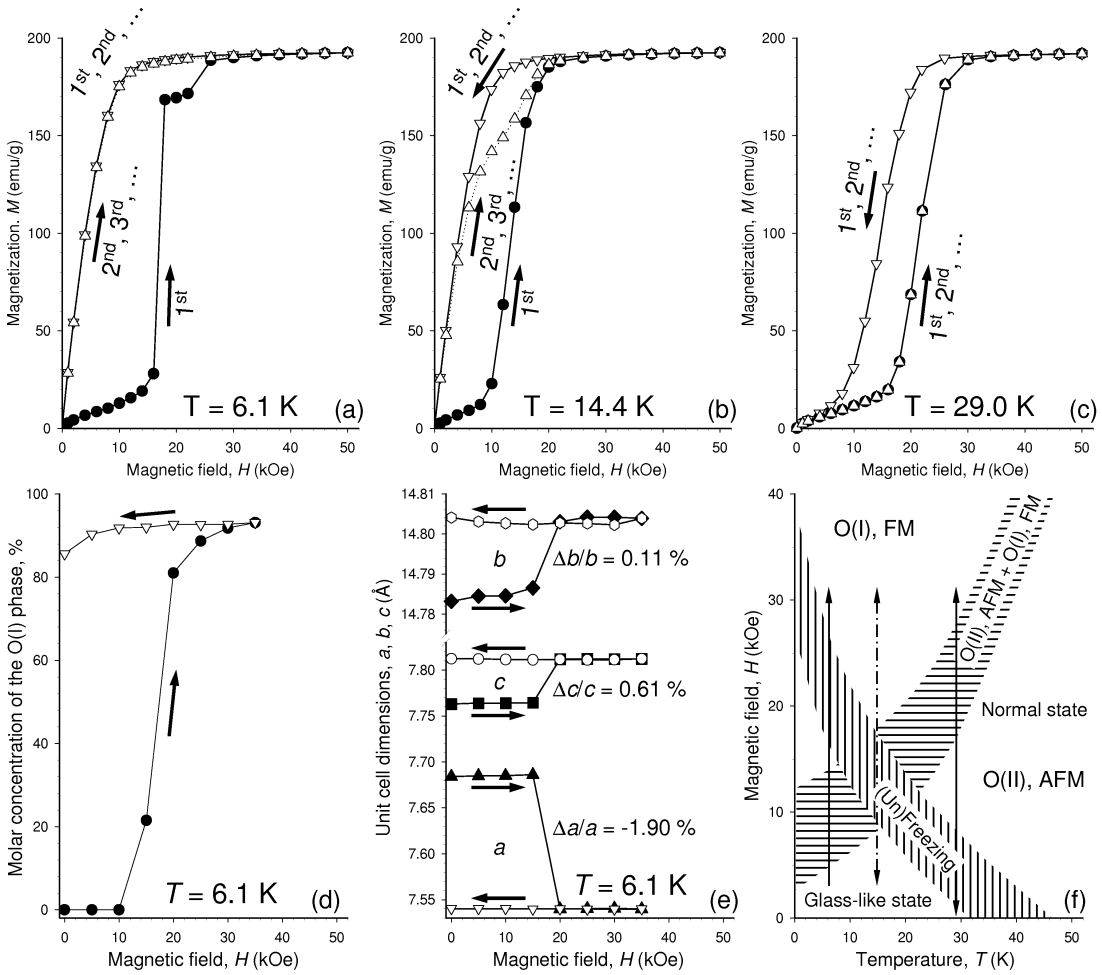

Fig. 10 The isothermal magnetization of polycrystalline, zero-field-cooled Gd_5Ge_4 measured at different temperatures illustrating the complete irreversibility (a), partial (b), and full (c) reversibility of the magnetic-field-induced metamagnetic transformation. The molar concentration of the O(I) phase (d) and unit cell dimensions of the majority phase (e), as functions of magnetic field determined from in situ X-ray powder diffraction data collected at the same temperature as in (a). The low-temperature, low-magnetic-field part of the Gd_5Ge_4 phase diagram in the temperature–magnetic field coordinates for the initial magnetization established from bulk magnetization and in situ X-ray powder diffraction data (f). The arrows in (a)–(e) indicate the directions of the magnetic field change. The arrows in (f) correspond to the three temperatures shown in (a), (b), and (c) illustrating how the reversibility of the O(II) AFM ↔ O(I) FM phase transition is affected by the glass-like phase-transition boundary.

reported recently in polycrystalline $Tb_5Si_2Ge_2$ [117]. The presence of these new magnetic states of Gd_5Ge_4 is reflected in the phase diagram depicted in Fig. 11. Unlike the negligible anisotropy of the true PM state above 240 K, the Griffiths phase-like Gd_5Ge_4 exhibits strong magnetic anisotropy, with the *b*-axis being clearly the direction with the largest magnetization. The latter is consistent with the same axis being the easy magnetization direction of the long-range ordered FM Gd_5Ge_4 phase. Signatures of the short-range FM correlations are easily suppressed by magnetic fields exceeding ~5 kOe. Microscopically, the formation of the Griffiths-like phase can be related to the competition of the interslab and intraslab magnetic exchange interactions that are present in a distinctly layered crys-

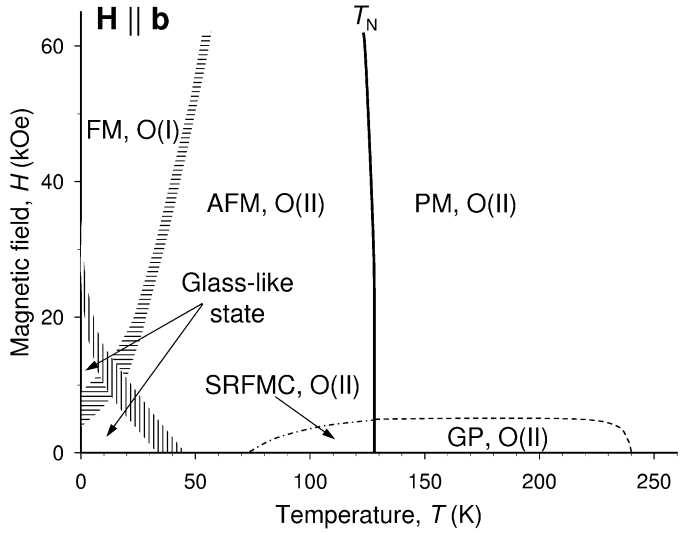

Fig. 11 The magnetic-phase diagram of Gd_5Ge_4 single crystal in temperature–magnetic field coordinates for the initial magnetization with the magnetic field vector parallel to the *b*-axis reflecting short-range FM correlations (SRFMC) below T_N and a Griffiths-like phase (GP) state above T_N.

tal structure of the compound. Macroscopically, the appearance of the Griffiths-like phase may be enhanced by the precipitates of thin plates of Gd_5Ge_3 [118] present in the sample.

ACKNOWLEDGMENT

This work is supported by the Office of Basic Energy Sciences, Materials Sciences Division of the U.S. Department of Energy under Contract No. DE-AC02-07CH11358 with Iowa State University.

REFERENCES AND NOTES

1. *Intermetallic* (adj.): composed of two or more metals or of a metal and a nonmetal; *intermetallic compound*: being an alloy having a characteristic crystal structure and usually a definite composition. Merriam-Webster On Line: <www.m-w.com>.
2. P. Villars. *Pearson's Handbook Desk Edition. Crystallographic Data for Intermetallic Phases*, ASM International, Materials Park, OH (1997).
3. P. I. Krypiakevich. *Structure Types of Intermetallic Compounds*, Nauka, Moscow (1977).
4. K. R. Andress, E. Alberti. *Z. Metallkd.* **27**, 126 (1935).
5. Z. Ban, M. Sikirica. *Acta Crystallogr.* **18**, 594 (1965).
6. J. B. Friauf. *J. Am. Chem. Soc.* **49**, 3107 (1927).
7. K. A. Gschneidner Jr., V. K. Pecharsky. *Z. Kristallogr.* **221**, 375 (2006).
8. F. Steglich, J. Aarts, C. D. Bredl, W. Leike, D. Meschede, W. Franz, H. Schaefer. *Phys. Rev. Lett.* **43**, 1892 (1979).
9. G. S. Smith, A. G. Tharp, Q. Johnston. *Nature (London)* **210**, 1148 (1966).
10. G. S. Smith, Q. Johnston, A. G. Tharp. *Acta Crystallogr.* **22**, 269 (1967).
11. G. S. Smith, A. G. Tharp, Q. Johnston. *Acta Crystallogr.* **22**, 940 (1967).
12. F. Holtzberg, R. J. Gambino, T. R. McGuire. *J. Phys. Chem. Solids* **28**, 2283 (1967).
13. S. Parviainen. *Phys. Status Solidi A* **60**, K13 (1980).
14. Yu. V. Serdyuk, R. P. Krentis. *VINITI 4230-81 (deposited document)*, 1-14 (1981).

15. J. M. Elbicki, L. Y. Zhang, R. T. Obermyer, W. E. Wallace, S. G. Sankar. *J. Appl. Phys.* **69**, 5571 (1991).
16. V. K. Pecharsky, K. A. Gschneidner Jr. *Phys. Rev. Lett.* **78**, 4494 (1997).
17. V. K. Pecharsky, K. A. Gschneidner Jr. *Appl. Phys. Lett.* **70**, 3299 (1997).
18. V. K. Pecharsky, K. A. Gschneidner Jr. *J. Magn. Magn. Mater.* **70**, L179 (1997).
19. V. K. Pecharsky, K. A. Gschneidner Jr. *J. Alloys Compd.* **260**, 98 (1997).
20. W. Choe, V. K. Pecharsky, A. O. Pecharsky, K. A. Gschneidner Jr., V. G. Young Jr., G. J. Miller. *Phys. Rev. Lett.* **84**, 4617 (2000).
21. A. Yu. Kozlov, V. V. Pavlyuk, V. M. Davydov. *Intermetallics* **12**, 151 (2004).
22. Yu. Mozharivskyj, W. Choe, A. O. Pecharsky, G. J. Miller. *J. Am. Chem. Soc.* **125**, 15183 (2003).
23. H. B. Wang, Z. Altounian, D. H. Ryan. *Phys. Rev. B* **66**, 214413 (2002).
24. H. B. Wang, M. Elouneg-Jamróz, D. H. Ryan, Z. Altounian. *J. Appl. Phys.* **93**, 8304 (2003).
25. H. B. Wang, Z. Altounian, D. H. Ryan. *J. Phys.: Condens. Matter* **16**, 3053 (2003).
26. J. C. P. Campoy, E. J. R. Plaza, A. Magnus, J. Carvalho, A. A. Coelho, S. Gama, P. J. von Ranke. *J. Magn. Magn. Mater.* **272–276**, 2375 (2004).
27. Y. G. Chen, T. B. Zhang, Y. B. Tang, M. J. Tu. *Proceedings of First International Conference on Magnetic Refrigeration at Room Temperature*, Montreux, Switzerland, 27–30 September 2005, P. Egolf, (Ed.), pp. 239–247, International Institute of Refrigeration, Paris (2005).
28. Z. Tiebang, C. Yungui, T. Yongbai, T. Mingjing. *J. Chin. RE Soc.* **23**, 409 (2005).
29. A. Guloy, J. D. Corbett. *J. Solid State Chem.* **178**, 1112 (2005).
30. T. Zhang, Y. Chen, Y. Tang, M. Tu. *J. Alloys Compd.* **422**, 25 (2006).
31. E. Zhang, Y. Chen, T. Zhang, Y. Tang, M. Tu. *J. Magn. Magn. Mater.* **305**, 410 (2006).
32. D. H. Ryan, M. Elouneg-Jamróz, J. van Lierop, Z. Altounian, H. B. Wang. *Phys. Rev. Lett.* **90**, 117202 (2003).
33. H. F. Yang, G. H. Rao, G. Y. Liu, Z. W. Ouyang, W. F. Liu, X. M. Feng, W. G. Chu, J. K. Liang. *J. Alloys Compd.* **368**, 248 (2004).
34. H. B. Wang, Z. Altounian, D. H. Ryan, J. M. Cadogan, I. P. Swainson. *J. Appl. Phys.* **97**, 10M506 (2005).
35. R. Nirmala, A. V. Morozkin, S. K. Malik. *Europhys. Lett.* **72**, 652 (2005).
36. A. Chernyshov, Ya. Mudryk, V. K. Pecharsky, K. A. Gschneidner Jr. *J. Appl. Phys.* **99**, 08Q102 (2006).
37. L. Morellon, J. Blasco, P. A. Algarabel, M. R. Ibarra. *Phys. Rev. B* **62**, 1022 (2000).
38. K. A. Gschneidner Jr., V. K. Pecharsky, A. O. Pecharsky, V. V. Ivtchenko, E. M. Levin. *J. Alloys Compd.* **303–304**, 214 (2000).
39. V. V. Ivtchenko, V. K. Pecharsky, K. A. Gschneidner Jr. *Adv. Cryog. Eng.* **46A**, 405 (2000).
40. Q. L. Liu, G. H. Rao, H. F. Yang, J. K. Liang. *J. Alloys Compd.* **325**, 50 (2001).
41. C. Ritter, L. Morellon, P. A. Algarabel, C. Magen, M. R. Ibarra. *Phys. Rev. B* **65**, 094405 (2002).
42. N. P. Thuy, N. V. Nong, N. T. Hien, L. T. Tai, T. Q. Vinh, P. D. Thang, E. Bruck. *J. Magn. Magn. Mater.* **242–245**, 841 (2002).
43. A. O. Pecharsky, K. A. Gschneidner Jr., V. K. Pecharsky, C. E. Schindler. *J. Alloys Compd.* **338**, 126 (2002).
44. H. F. Yang, G. H. Rao, W. G. Chu, G. Y. Liu, Z. W. Ouyang, J. K. Liang. *J. Alloys Compd.* **339**, 189 (2002).
45. H. F. Yang, G. H. Rao, G. Y. Liu, Z. W. Ouyang, W. F. Liu, X. M. Feng, W. G. Chu, J. K. Liang. *J. Alloys Compd.* **346**, 190 (2002).
46. H. Huang, A. O. Pecharsky, V. K. Pecharsky, K. A. Gschneidner Jr. *Adv. Cryog. Eng.* **47A**, 11 (2002).
47. H. F. Yang, G. H. Rao, G. Y. Liu, Z. W. Ouyang, W. F. Liu, X. M. Feng, W. G. Chu, J. K. Liang. *J. Magn. Magn. Mater.* **263**, 146 (2003).
48. A. O. Pecharsky, K. A. Gschneidner Jr., V. K. Pecharsky. *J. Magn. Magn. Mater.* **267**, 60 (2003).

49. W. Choe, A. O. Pecharsky, M. Woerle, G. J. Miller. *Inorg. Chem.* **42**, 8223 (2003).
50. H. F. Yang, G. H. Rao, G. Y. Liu, Z. W. Ouyang, W. F. Liu, X. M. Feng, W. G. Chu, J. K. Liang. *J. Alloys Compd.* **348**, 150 (2003).
51. A. O. Pecharsky, K. A. Gschneidner Jr., V. K. Pecharsky, D. L. Schlagel, T. A. Lograsso. *Phys. Rev. B* **70**, 144419 (2004).
52. A. O. Pecharsky, V. K. Pecharsky, K. A. Gschneidner Jr. *J. Alloys Compd.* **379**, 127 (2004).
53. K. Ahn, A. O. Tsokol, Yu. Mozharivskyj, K. A. Gschneidner Jr., V. K. Pecharsky. *Phys. Rev. B* **72**, 054404 (2005).
54. J. Vejpravová, J. Prokleáka, S. Daniš, V. Sechovský. *Physica B* **378–380**, 784 (2006).
55. J. Prokleáka, J. Vejpravová, S. Daniš, V. Sechovský. *Physica B* **378–380**, 1111 (2006).
56. A. O. Tsokol, K. A. Gschneidner Jr., V. K. Pecharsky. Unpublished.
57. K. Ahn, K. A. Gschneidner Jr., V. K. Pecharsky. *Phys. Rev. B* (2007). To be published.
58. R. Vijaraghavan, A. O. Tsokol, K. A. Gschneidner Jr., V. K. Pecharsky. Unpublished.
59. H. U. Pfeifer, K. Schubert. *Z. Metallkd.* **57**, 884 (1966).
60. P. I. Kripyakevicn, V. A. Yartys. *Dopov. Akad. Nauk Ukr. RSR. Ser. A* **37**, 1129 (1975).
61. L. Morellon, P. A. Algarabel, M. R. Ibarra, J. Blasco, García-Landa, Z. Arnold, F. Albertini. *Phys. Rev. B* **58**, R14721 (1998).
62. A. O. Pecharsky, K. A. Gschneidner Jr., V. K. Pecharsky. *J. Appl. Phys.* **93**, 4722 (2003).
63. V. K. Pecharsky, G. D. Samolyuk, V. P. Antrropov, A. O. Pecharsky, K. A. Gschneidner Jr. *J. Solid State Chem.* **171**, 57 (2003).
64. K. A. Gschneidner Jr. *J. Alloys Compd.* **193**, 1 (1993).
65. C. J. Voyer, D. H. Ryan, K. Ahn, K. A. Gschneidner Jr., V. K. Pecharsky. *Phys. Rev. B* **73**, 174422 (2006).
66. G. J. Miller. *Chem. Soc. Rev.* **35**, 799 (2006).
67. V. K. Pecharsky, K. A. Gschneidner Jr. *Adv. Mater. (Weinheim)* **13**, 683 (2001).
68. O. Tegus, E. Brück, L. Zhang, Dagula, K. H. J. Buschow, F. R. de Boer. *Physica B* **319**, 174 (2002).
69. E. M. Levin, K. A. Gschneidner Jr., T. A. Lograsso, D. L. Schlagel, V. K. Pecharsky. *Phys. Rev. B* **69**, 144428 (2004).
70. C. Magen, L. Morellon, P. A. Algarabel, M. R. Ibarra, Z. Arnold, J. Kamarad, T. A. Lograsso, D. L. Schlagel, V. K. Pecharsky, A. O. Tsokol, K. A. Gschneidner Jr. *Phys. Rev. B* **72**, 024416 (2005).
71. Z. W. Ouyang, V. K. Pecharsky, K. A. Gschneidner Jr., D. L. Schlagel, T. A. Lograsso. *Phys. Rev. B* **74**, 024401 (2006).
72. L. Tan, A. Kreyssig, J. W. Kim, A. I. Goldman, R. J. McQueeney, D. Wermeille, B. Sieve, T. A. Lograsso, D. L. Schlagel, S. L. Budko, V. K. Pecharsky, K. A. Gschneidner Jr. *Phys. Rev. B* **71**, 214408 (2005).
73. J. S. Leib, C. C. H. Lo, J. E. Snyder, D. C. Jiles, V. K. Pecharsky, D. S. Schlagel, T. A. Lograsso. *IEEE Trans. Magn.* **38**, 2447 (2002).
74. G. D. Samolyuk, V. P. Antropov. *J. Appl. Phys.* **91**, 8540 (2002).
75. B. N. Harmon, V. N. Antonov. *J. Appl. Phys.* **91**, 9815 (2002).
76. B. N. Harmon, V. N. Antonov. *J. Appl. Phys.* **93**, 4678 (2003).
77. G. D. Samolyuk, V. P. Antropov. *J. Appl. Phys.* **93**, 6882 (2002).
78. H. Tang, V. K. Pecharsky, G. D. Samolyuk, M. Zou, K. A. Gschneidner Jr., V. P. Antropov, D. L. Schlagel, T. A. Lograsso. *Phys. Rev. Lett.* **93**, 237203 (2004).
79. G. D. Samolyuk, V. P. Antropov. *J. Appl. Phys.* **97**, 10A310 (2005).
80. D. Paudyal, V. K. Pecharsky, K. A. Gschneidner Jr., B. N. Harmon. *Phys. Rev. B* **73**, 144406 (2006).
81. A. O. Pecharsky, V. K. Pecharsky, K. A. Gschneidner Jr. *J. Alloys Compd.* **344**, 362 (2002).

82. Y. Mozharivskyj, A. O. Pecharsky, V. K. Pecharsky, G. J. Miller. *J. Am. Chem. Soc.* **127**, 317 (2005).
83. L. Morellon, J. Stankiewicz, B. García-Landa, P. A. Algarabel, M. R. Ibarra. *Appl. Phys. Lett.* **73**, 3462 (1998).
84. E. M. Levin, V. K. Pecharsky, K. A. Gschneidner Jr. *Phys. Rev. B* **60**, 7993 (1999).
85. E. M. Levin, V. K. Pecharsky, K. A. Gschneidner Jr., P. Tomlinson. *J. Magn. Magn. Mater.* **210**, 181 (2000).
86. L. Morellon, P. A. Algarabel, C. Magen, M. R. Ibarra. *J. Magn. Magn. Mater.* **237**, 119 (2001).
87. E. M. Levin, A. O. Pecharsky, V. K. Pecharsky, K. A. Gschneidner Jr. *Phys. Rev. B* **63**, 064426 (2001).
88. E. M. Levin, V. K. Pecharsky, K. A. Gschneidner Jr., G. J. Miller. *Phys. Rev. B* **64**, 235103 (2001).
89. E. M. Levin, V. K. Pecharsky, K. A. Gschneidner Jr. *Phys. Rev. B* **63**, 174110 (2001).
90. M. Zou, H. Tang, D. L. Schlagel, T. A. Lograsso, K. A. Gschneidner Jr., V. K. Pecharsky. *J. Appl. Phys.* **99**, 08B304 (2006).
91. J. B. Sousa, M. E. Braga, F. C. Correía, F. Carpinteiro, L. Morellon, P. A. Algarabel, M. R. Ibarra. *Phys. Rev. B* **67**, 134416 (2003).
92. F. Casanova, A. Labarta, X. Batlle, F. J. Pérez-Reche, E. Vives, L. Mañosa, A. Planes. *Appl. Phys. Lett.* **86**, 262504 (2005).
93. J. B. Sousa, A. M. Pereira, F. C. Correia, J. M. Teixeira, J. P. Araújo, R. P. Pinto, M. E. Braga, L. Morellon, P. A. Algarabel, C. Magen, M. R. Ibarra. *J. Phys.: Condens. Matter* **17**, 2461 (2005).
94. M. Manekar, M. K. Chattopadhyay, R. Kaul, V. K. Pecharsky, K. A. Gschneidner Jr. *J. Phys.: Condens. Matter* **18**, 6017 (2006).
95. F. Casanova, A. Labarta, X. Batlle, E. Vives, J. Marcos, L. Mañosa, A. Planes. *Eur. Phys. J. B* **40**, 427 (2004).
96. J. Leib, J. E. Snyder, T. A. Lograsso, D. Schlagel, D. C. Jiles. *J. Appl. Phys.* **95**, 6915 (2004).
97. V. Hardy, S. Majumdar, S. J. Crowe, M. R. Lees, D. McK. Paul, L. Hervé, A. Maignan, S. Hébert, C. Martin, C. Yaicle, M. Herviue, B. Raveau. *Phys. Rev. B* **69**, 020407(R) (2004).
98. J. D. Moore, G. K. Perkins, Y. Bugoslavsky, M. K. Chattopadhyay, S. B. Roy, P. Chaddah, V. K. Pecharsky, K. A. Gschneidner Jr., L. F. Cohen. *Appl. Phys. Lett.* **88**, 072501 (2006).
99. J. D. Moore, G. K. Perkins, Y. Bugoslavsky, L. F. Cohen, M. K. Chattopadhyay, S. B. Roy, P. Chaddah, K. A. Gschneidner Jr., V. K. Pecharsky. *Phys. Rev. B* **73**, 144426 (2006).
100. F. Casanova, A. Labarta, X. Batlle. *Phys. Rev. B* **72**, 172402 (2005).
101. F.-J. Pérez-Reche, F. Casanova, E. Vives, L. Mañosa, A. Planes, J. Marcos, X. Batlle, A. Labarta. *Phys. Rev. B* **73**, 014110 (2006).
102. S. B. Roy, M. K. Chattopadhyay, P. Chaddah, J. D. Moore, G. K. Perkins, L. F. Cohen, K. A. Gschneidner Jr., V. K. Pecharsky. *Phys. Rev. B* **74**, 012403 (2006).
103. V. K. Pecharsky, K. A. Gschneidner Jr. In *Magnetism and Structure in Functional Materials*, A. Planes, L. Mañosa, A. Saxena (Eds.), pp. 199–222, Springer-Verlag, Berlin (2007).
104. V. K. Pecharsky, A. P. Holm, K. A. Gschneidner Jr., R. Rink. *Phys. Rev. Lett.* **91**, 197204 (2003).
105. V. K. Pecharsky, K. A. Gschneidner Jr. *J. Magn. Magn. Mater.* **200**, 44 (1999).
106. S. Misra, G. J. Miller. *J. Solid State Chem.* **179**, 2290 (2006).
107. J. Szade, G. Skorek. *J. Magn. Magn. Mater.* **196–197**, 699 (1999).
108. E. M. Levin, K. A. Gschneidner Jr., V. K. Pecharsky. *Phys. Rev. B* **65**, 214427 (2002).
109. C. Magen, L. Morellon, P. A. Algarabel, C. Marquina, M. R. Ibarra. *J. Phys.: Condens. Matter* **15**, 2389 (2003).
110. F. Casanova, A. Labarta, X. Batlle, J. Marcos, L. Mañosa, A. Planes, S. de Brion. *Phys. Rev. B* **69**, 104416 (2004).
111. F. Casanova, S. de Brion, A. Labarta, X. Batlle. *J. Phys. D: Appl. Phys.* **38**, 3343–3347 (2005).
112. A. P. Holm, V. K. Pecharsky, K. A. Gschneidner Jr., R. Rink, M. N. Jirmanus. *Rev. Sci. Instrum.* **75**, 1081 (2004).

113. Ya. Mudryk, A. P. Holm, K. A. Gschneidner Jr., V. K. Pecharsky. *Phys. Rev. B* **72**, 064442 (2004).
114. H. Tang, V. K. Pecharsky, K. A. Gschneidner Jr., A. O. Pecharsky. *Phys. Rev. B* **69**, 064410 (2004).
115. Z. W. Ouyang, V. K. Pecharsky, K. A. Gschneidner Jr., D. L. Schlagel, T. A. Lograsso. *Phys. Rev. B* **74**, 094404 (2006).
116. R. B. Griffiths. *Phys. Rev. Lett.* **23**, 17 (1969).
117. C. Magen, P. A. Algarabel, L. Morellon, J. P. Araújo, C. Ritter, M. R. Ibarra, A. M. Pereira, J. B. Sousa. *Phys. Rev. Lett.* **96**, 167201 (2006).
118. O. Ugurlu, L. S. Chumbley, D. L. Schlagel, T. Lograsso. *Acta Mater.* **54**, 1211 (2006).